IUBAT Review—A Multidisciplinary Academic Journal, 8(2): 45-58
https://doi.org/10.3329/iubatr.v8i2.86874

Numerical Investigation of Parallel-Plate Counter Flow Heat Exchanger: An Approximation using the Finite Element Method

Md. Moniruzzaman Bhuyan[1*], Dilara Dilshad[2], Mashky Chowdhury Surja[3]

[1]*Department of Mathematics, International University of Business Agriculture and Technology (IUBAT), Dhaka, Bangladesh, ORCID:0009-0007-7070-1960*
[2]*Department of English and Modern Languages, International University of Business Agriculture and Technology (IUBAT), Dhaka, Bangladesh, ORCID:0009-0002-0714-1511*
[3]*School of Science, Engineering and Technology East Delta University, Chittagong, Bangladesh, ORCID:0009-0001-9009-1561*

Keywords:

Counter Flow; Finite Element Method; Heat Exchanger; Numerical Simulation; Parallel Plate.

Abstract

Heat exchangers are widely employed in various sectors for both heating and cooling. This paper describes a numerical model for simulating a counter-flow parallel plate heat exchanger. The computational domain was a representative unit cell of a multi-channel heat exchanger, which included a hot channel and a cold channel separated by plates. The simulation is directed in COMSOL for an oil-to-water heat exchanger, with hot oil and cold water flowing in opposing directions through distinct channels. This study displays temperature distributions in cold and hot channels with different inlet and outlet temperatures (293.15-340 K and 300-330 K). For 293.15-340 K, the hot channel temperature decreased from 340 K to 317.8 K, while the cold channel temperature increased from 293.15 K to 316 K. At 50 mm, the temperature gradient (K/m) is examined, and at 200 mm, the highest pressure of 0.0715 Pa is found. The hot channel displays a vorticity magnitude of 8.9275 s^{-1}, while the cold channel has 0.0178 s^{-1}. Simulations using finer meshes resulted in greater temperature accuracy. The LMTD values are 23.46 (293.15-340 K) and 15.02 (300-330 K), with an efficiency of 0.85 for NTU 1.5. The model assists in optimizing heat exchanger design effectively.

1. Introduction

Parallel-plate heat exchangers are widely used in several industries, including chemical, pharmaceutical, and food processing. They have recently been used in innovative thermal engineering applications. As an example, they are now used in small-scale reaction systems which include gas-phase reactions and solid catalysts (Hardt, Ehrfeld & Hessel, 2003). Thermoelectric generators convert low-grade thermal energy into electricity (Esarte, Min & Rowe, 2001; Yu & Zhao, 2007), as do acoustic engines and refrigerators (Wakeland & Keoliana, 2004). Furthermore,

*Corresponding author's E-mail address: bhuyan.qs@iubat.edu
Article received: April 2025 Revised and accepted: November 2025 Published: December 2025

they perform an important role in several cryogenic systems (Marquardt & Radebaugh, 2003; Nellis, 2003; Radebaugh, 2005).

Parallel-plate heat exchangers have seen substantial advancements in analysis due to their simple design and defined flow conditions (Shah & London, 1978). Specifically, the analysis of the steady-state laminar heat transfer among various streams coupled through compatibility criteria at the boundaries represents the so-called conjugated Graetz problem (Papoutsakis & Ramkrishna, 1981a, 1981b; Perelman, 1961). Under certain assumptions, such as constant fluid properties and fully developed laminar flow, the problem becomes linear and can be solved using eigenfunction expansions. In counterflow systems, eigenfunctions indicate positive and negative eigenvalues (Papoutsakis & Ramkrishna, 1981b; Nunge & Gill, 1966).

Jia *et al*. (2014) used a 3D model of a multilayered counterflow parallel heat exchanger to simulate heat transfer and fluid flow in a unit cell with one cold and one hot channel. The model was simulated in COMSOL, using oil and water as working fluids. The temperature, velocity, and pressure distributions in the channels may assist in optimizing heat exchanger design (Jia, Hu, & Elbalsohi, 2014).

Jia *et al*. (2014) provided a simulation model to evaluate the performance of a counterflow plate-fin heat exchanger. Their study applied a 3D model of a counterflow plate-fin heat exchanger to simulate heat transfer and fluid flow in a unit cell with one hot and one cold channel. Using COMSOL 4.3b with oil and water as working fluids, the model produced detailed temperature and velocity distributions to aid the understanding of heat transfer behavior. The calculated hydrodynamic and thermal entrance lengths agreed well with the theoretical values. A parametric analysis looked at how channel length affected temperature distribution, heat transfer effectiveness, and pressure drop. The model provides a solid framework for improving comparable heat exchanger designs (Jia, Hu & Xiong, 2014).

Piroozfam *et al.* (2018) investigated three methods to enhance heat transfer in counter-flow heat exchangers. Their study demonstrates that obstacle forms and flow adjustments can considerably increase the performance of a Compact Flat-plate Heat Exchanger (CFHE). Rectangular and edge barriers provide the most thermal increase (up to 18%), while semicircular ones produce the least. Corrugated plates and pulsating flows improve heat transfer, although excessive waves may diminish efficiency. Using an elastic plate with pulsed cold flow improves overall performance by 40-50% (Piroozfam, Hosseinpour Shafaghi & Razavi, 2018).

In recent years, computational fluid dynamics (CFD) analysis has become more prevalent in heat exchanger design and performance evaluations, specifically for examining thermal performance, effectiveness, and temperature distributions. This study analyses heat transfer due to fluid flow within a multilayered circular tubes of radius 30μm and length 400μm within counter-flow parallel-plate heat exchanger.

The investigation focuses on temperature distribution and heat transfer rates to determine the system's performance. This finding has practical implications in the engineering field, as the use of such systems is becoming more widespread. The use of a 400 mm channel, which has not been previously investigated, is one of the study's distinguishing features. The paper can be useful for measuring accuracy in this specific subject. In this study, Finite Element-based software COMSOL MULTIPHYSICS is utilized, which is currently prominent in this research area.

2. Governing Equations

For this simulation, Computational Fluid Dynamics (CFD) was utilized to determine fluid behavior and anticipate fluid dynamical procedures in this model. In general, the CFD method is mathematically solved by applying the Navier-Stokes equations to every finite element of the computational domain. The non-isothermal laminar flow model is additionally employed in this simulation. The continuity equation, Navier-Stokes equations, and energy equation are identified by the equations listed below (COMSOL, n.d.; Cook, 1995; Löhner, 1987; Bhuyan *et, al*. 2025, Bhuyan *et, al*. 2024, S. Acherjee *et. al*, 2020, Bhuyan *et, al*. 2017).

$$\frac{\partial \rho}{\partial t} + \nabla \cdot (\rho \mathbf{u}) = 0 \tag{1}$$

$$\rho(\boldsymbol{u}.\nabla)\boldsymbol{u} + \rho\frac{\partial u}{\partial t} = \nabla.[-p\boldsymbol{I} + \mu(\nabla\mathbf{u} + (\nabla\mathbf{u})^{T})] - \frac{2}{3}\mu(\nabla.\boldsymbol{u})\boldsymbol{I} - \frac{2}{3}\rho K\boldsymbol{I}] + \boldsymbol{F} \tag{2}$$

The heat transfer rate through a fluid is determined by the following equation:

$$\rho C_p\left(\frac{\partial T}{\partial t} + (\boldsymbol{u}.\nabla \mathrm{T})\right) = \nabla \cdot (k\nabla T) + Q \tag{3}$$

If the velocity is to zero the equation becomes

$$\rho C_p \frac{\partial T}{\partial t} + \nabla \cdot (-k\nabla T) = \mathbf{Q} \tag{4}$$

The log mean temperature difference (LMTD) is calculated using the following equation (Zavala-Río & Santiesteban-Cos, 2004).

$$LMTD = \frac{(T_1 - t_2) - (T_2 - t_1)}{\ln \dfrac{(T_1 - t_2)}{(T_2 - t_1)}} \tag{5}$$

Where T_1 hot stream inlet temperature, T_2 hot stream outlet temperature, t_1 cold stream inlet temperature, and t_2 cold stream outlet temperature are specified.

2.1 Boundary conditions

In the boundary section, the following equations define the inlet conditions for hot and cold water, the pressure outlet, and the condition of no viscous stress:

$$p = p_o \tag{6}$$

$$[\mu(\nabla \mathbf{u} + (\nabla \mathbf{u})^T)] - \frac{2}{3}\mu(\nabla . \boldsymbol{u})\boldsymbol{I}]\boldsymbol{n} = 0 \tag{7}$$

$$\mathbf{u} \cdot \mathbf{n} = 0 \tag{8}$$

$$T = T_2 = 300 \tag{9}$$

$$T = T_1 = 330 \tag{10}$$

3. Computational domain and mesh generation

This is a model of an oil-to-water heat exchanger. The radius of the channel is 30 µm. The channels measure 50 x 150 x 400 µm. Table 3.1 shows the key parameters used in this simulation. Oil and water are considered as fluids in this simulation. Table 3.1 shows the parameters of water at 26.85K and oil at 56.85K, which were used to determine Reynolds numbers for each channel. The cold and hot channels have Reynolds numbers of 998 and 354, respectively. The problem was addressed numerically using the software COMSOL MULTIPHYSICS. Figure 3.2 displays an unstructured mesh with 33537 tetrahedral elements. The simulations were done on a laptop with Intel Core i7 CPUs and 8 GB of RAM.

Table 3.1: Numerical Parameters

Description	Name	Expression	Value
Channel radius	R	µm	30
Mean velocity	V_mean	mm/s	2.5
Temperature (hot channel)	T_hot	K	330
Temperature (cold channel)	T_cold	K	300
Mean temperature	T_mean	K	315
Fluid density	rho	Kg/m^3	1000

Table 3.2: Mesh design

Description	Fine mesh	Finer mesh
Tetrahedral elements	31329	33537

Triangular elements	6474	6726
Edge elements	532	540
Elements of Vertex	24	24
Quality of Minimum Elements	0.07539	0.09283
Quality of Average Elements	0.7097	0.7175
Element Volume Ratio	0.01894	0.01754

The computational domain is seen in Figure 3. Figure 3(a) depicts the computational full domain, whereas Figure 3(b) shows the mesh design for the inlet and outlet, and Figure 3(c) displays the full domain mesh design. In Figure 3(b), blue color denotes a cold fluid channel, while red signifies a hot fluid channel.

A fine mesh design is used to evaluate the outcomes of the domain analysis. To improve simulation performance, the mesh design is constantly revised and changed. However, due to constraints in the computer's configuration and processing capacity, only the fine mesh is finally employed for calculation.

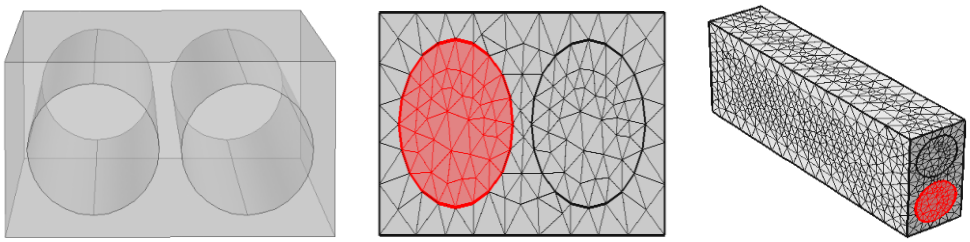

(a) (b) (c)

Figure 3: The computational domain with (a) a schematic diagram, (b) a cross-section of the mesh design, and (c) the mesh design of the full domain.

4. Simulation Setup

To simulate complicated geometries, computational simulations were performed utilizing the Finite Element Method (FEM) with tetrahedral elements. The primary goal of the numerical model is to examine heat transfer enhancement in a counter-flow parallel plate heat exchanger. A non-isothermal laminar flow model was used, taking into account the exchanger's particular geometric shape. The simulators account for time-dependent variations, although tube thickness is ignored for simplicity. In this setup, oil and water serve as working fluids in a counter-flow arrangement. A series of numerical simulations have been carried out using the parallel plate heat exchanger model to examine the effect of counter-flow on the heat transfer process.

4.1 Numerical Results

The major goal of this mathematical model is to enhance heat transmission within a rectangular plate subjected to non-isothermal laminar flow. This improvement is achieved by including a micro-strip designed to increase thermal performance. A

time-dependent simulation model is implemented to examine heat transfer behavior. For the purpose of this investigation, the tube's boundary conditions are assumed to maintain a constant temperature close to the water domain layer. Both oil and water are applied as working fluids for examining the effects of hot and cold channels on heat transfer processes. Simulations are conducted at a variety of temperature ranges ranging from 293.15 K to 340 K, with a particular focus on the 300 K–330 K range.

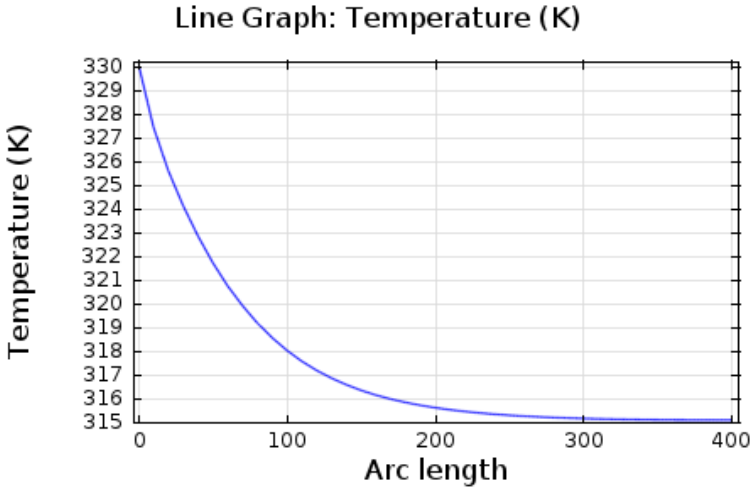

(a)

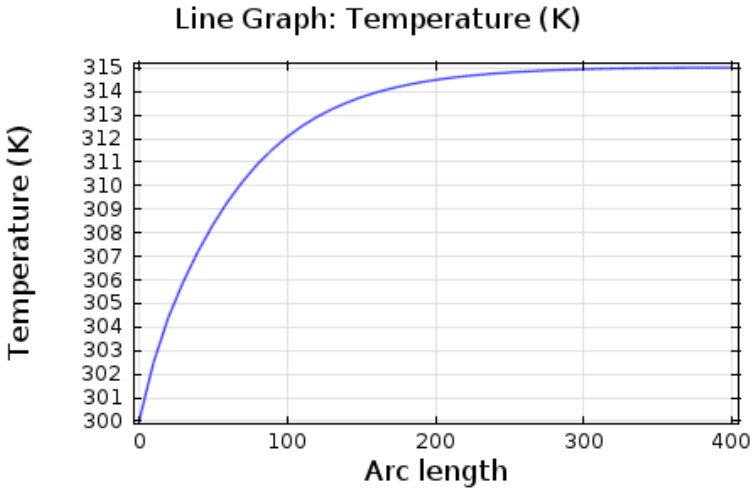

(b)

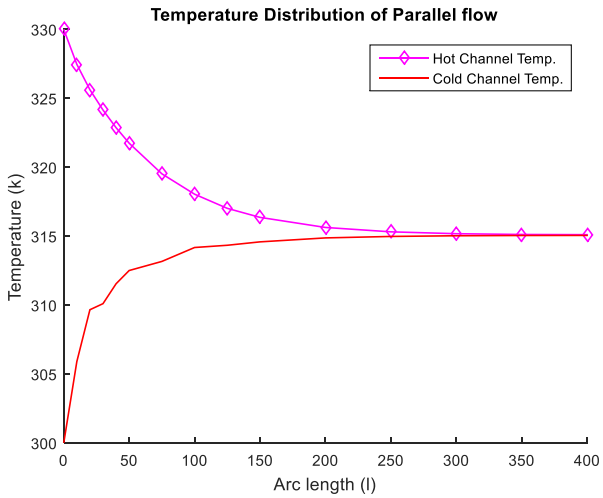

(c)

Figure 4.1: Temperature distribution along with arc length (a) Hot channel inlet to outlet (b) Cold channel inlet to outlet (c) Combined hot and cold temperature distribution.

In this study, Figures 4.1 (a), (b), and (c) demonstrate the temperature distribution along the arc length of the computational domain. Figure 4.1(a) indicates the distribution of the hot channel inlet to outlet. It is showing a gradual drop in temperature from 330 K at the inlet to about 315.1037 K at the outlet, resulting in a temperature variation of approximately 14.8963 K. On the other hand, Figure 4.1(b) depicts the temperature distribution in the cold channel, where the temperature increases gradually from 300 K to approximately 315.0486 K, indicating a variation of 15.0486 K. Figure 4.1(c) is showing the combined result of parallel flow. The pink color legend represents the hot channel temperature, which is decreasing downward, while the red color legend represents the cold channel temperature, which is increasing upward. The figure concludes by showing that the temperature of the hot and cold channels coincides at 300 mm on the arc length, which ranges from 0 to 400 mm.

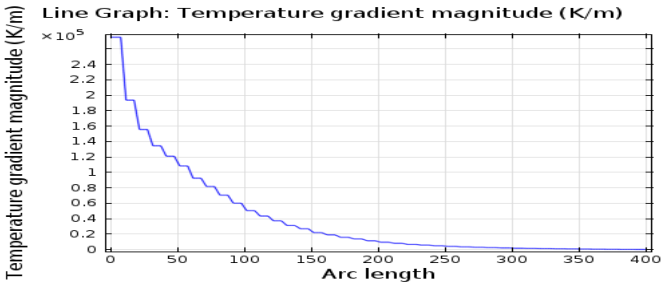

Figure 4.2: Temperature Gradient Magnitude

Figure 4.2 shows the temperature gradient magnitude (K/m), which decreases as the arc length increases and shows some variability. From the inlet to 50 mm, the temperature drops down sharply along the arc length. Again, it is declining moderately after 50 mm up to 250 mm, and finally, it is decreasing slowly till the arc length of 400 mm.

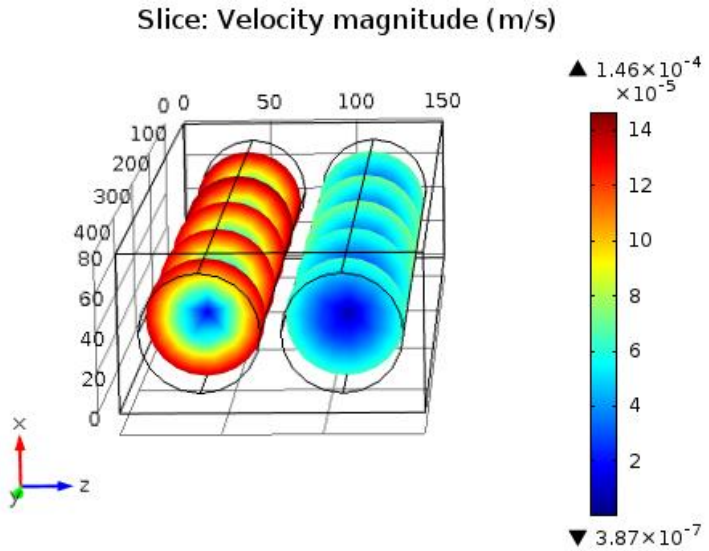

Figure 4.3: Velocity Magnitude

Figure 4.3 depicts the velocity magnitude (m/s) of a two-dimensional temperature slice from both the hot and cold channels. The velocity in the hot channel decreases gradually from the surface level to the central part. However, in the cold channel, the velocity increases from the surface area to the central point.

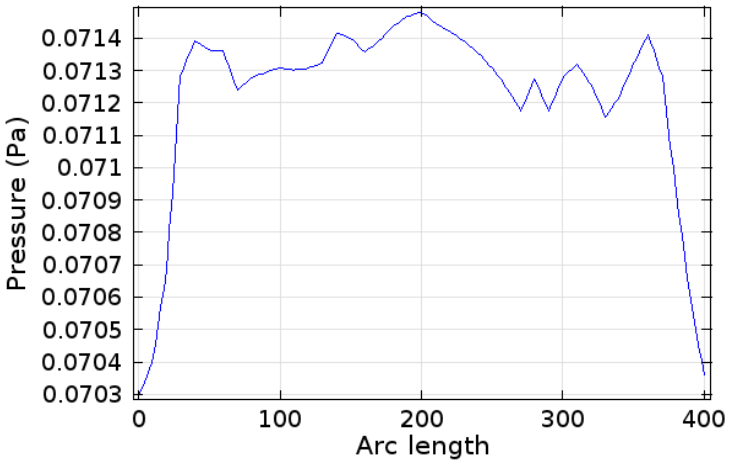

Figure 4.4: Pressure distribution along arc length

In Figure 4.4, the pressure drop is denoted along with the length. Some fluctuations of pressure drop from inlet to outlet are found as zero normal stress in the outlet is applied. This figure shows that the pressure is gradually decreasing from the inlet and suddenly increasing at particular arc length positions through some fluctuations. The pressure rises to its maximum at 300 mm, after which it drops sharply to 400 mm again.

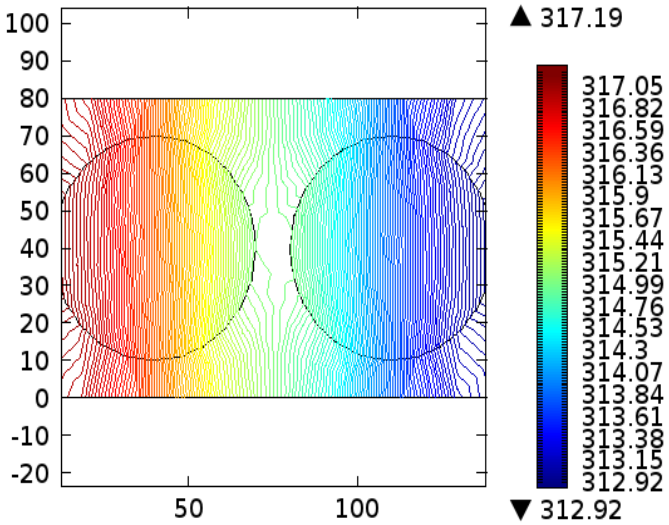

Figure 4.5 (a): cold channel contour temperature distribution

Figure 4.5 (a) depicts the cut plane of the cold channel at coordinates [50, 0, 0] µm, showing a progressive increase in temperature. Initially, the temperature in the cold channel is 312.92 K, rising to 317.19 K towards the end. Notably, the cold channel's original temperature at the beginning of the experiment was 300 K, showing an overall increase of 17.05 K. In contrast, the hot channel, which had a temperature of 330 K at the initial stage of the experiment, has significantly decreased. In this figure, the temperature has dropped by 12.81 K.

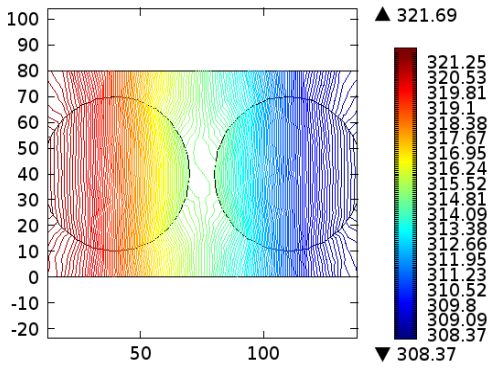

Figure 4.5 (b): hot channel contour temperature distribution

Figure 4.5(b) displays the cut plane of the hot channel at positions [120,0,0] µm, demonstrating an ongoing decrease in temperature. The starting temperature in the hot channel is 321.25 K, which drops to 308.37 K at the final point. Specifically, the hot channel's original temperature at the start of the experiment was 330 K, resulting in a 21.63 K reduction. In contrast, the temperature of the cold channel begins at 308.37 K and ends at 321.25 K, which, having been 300 K at the start of the experiment has dramatically increased by 21.69 K.

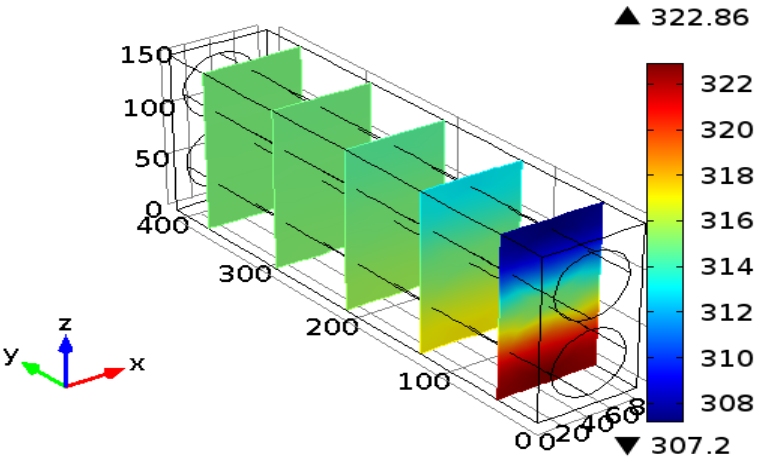

Figure 4.6: Temperature slice

In Figure 4.6, the hot channel's temperature falls gradually, while the cold channel's temperature improves continuously. The temperature in the inlet is 322.86 K for the hot channel and 307.2 K for the cold channel, along with the temperature of the hot channel falling and rising for the cold channel gradually. This figure indicates that the temperature of the hot and cold channels coincides between 314 K and 316 K.

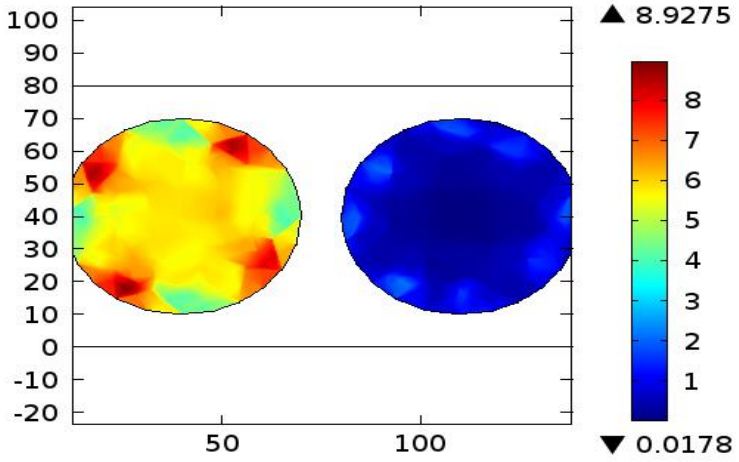

Figure 4.7: Vorticity magnitude

At the cut-plane position of (50, 0, 0) µm, the vorticity magnitude in the cold channel is 0.0178, while in the hot channel it is 8.9275. As a result, the vorticity magnitude is greater in the hot channel than in the cold.

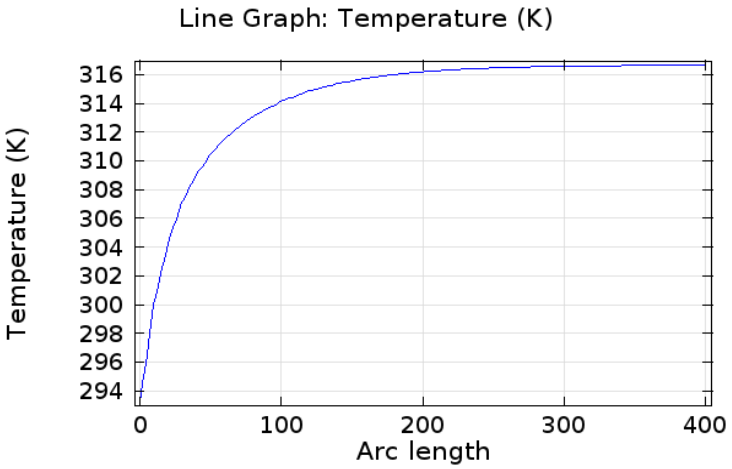

Figure 4.8:(a) cold channel

Figure 4.8 (a) depicts the temperature variation along the cold channel. Initially, the temperature is approximately 293.15 K. Between the arc lengths of 0 and 100 mm, the temperature rises dramatically to around 314 K. From 100 to 200 mm, it rises to nearly 316 K, indicating an almost 2 K increase from the previous stage. Between 200 and 300 mm, the temperature slowly rises, and between 300 and 400 mm, it is a sort of constant condition.

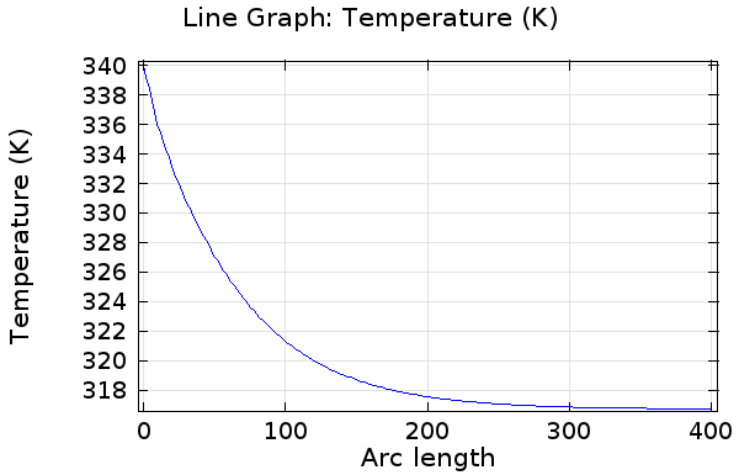

Figure 4.9: (b) hot channel

Figure 4.9(b) demonstrates the temperature variation along the hot channel. In general, the starting temperature is around 340 K. Between arc lengths of 0 and 100

mm, the temperature drops sharply, reaching about 321 K. From 100 to 200 mm, it reduces to almost 317.8 K; between 200 and 300 mm, the temperature gradually declines; and between 300 and 400 mm, it remains consistent.

Conclusion

A three-dimensional (3D) model of a multi-cell counter-flow parallel plate heat exchanger has been generated for this research in order to simulate fluid flow patterns and heat transfer and the enhancement of heat transfer for cold and hot channels. The simulations were performed using COMSOL Multiphysics, utilizing oil and water as working fluids. The main findings of the study are presented below:

- The simulation shows temperature distribution along the arc length for both cold and hot channels. The cold channel's temperature rises while the hot channel's temperature falls, with both temperatures eventually converging at a certain point. The study examined temperature variations in both cold and hot channels. Simulation with varying inlet temperatures from 293.15 to 340 K and from 300 to 330 K revealed consistent temperature behavior. For the hot channel (293.15-340 K), the temperature is gradually decreasing from 340 K to 317.8 K. For the cold channel (293.15-340 K), the temperature is gradually increasing from 293.15 K to 316 K.

- The study focuses on temperature gradient magnitude 1.1×10^{5} (K/m) in the position of 50 mm, which provides information on the rate of temperature change per unit length.
- The pressure drop from inlet to outlet has been measured in both channels. In the position of 200 mm, the maximum pressure remains, that is 0.0715 Pa.
- Vorticity magnitude is assessed to better understand the fluid flow dynamics: 8.9275 (1/s) for the hot channel and 0.0178 (1/s) for the cold channel.
- Simulations were performed with fine and finer mesh settings. Although the results were similar, the finer mesh produced somewhat better accuracy in temperature prediction. Only the finer mesh result is calculated in this study.
- LMTD value is 23.46 for the temperature of 293.15-340 K and 15.02 for the temperature of 300-330 K.

- The effectiveness 0.85 for the number of transfer units (NTU) 1.5 is found in this study (Onufrena *et al.*, 2022).

Future work may include simulation/experimental work on multilayer heat exchangers with extra fine mesh with increased pipe length.

Acknowledgment

The authors are grateful to Miyan Research Institute and Simulation Lab at International University of Business Agriculture and Technology. They would like to thank East Delta University for their assistance.

References

Bhuyan, M. M. & Deb, Ujjwal Kumar & Shahriar, M. & Acherjee, Simul. (2017). Simulation of Heat Transfer in a Tubular Pipe Using Different Twisted Tape Inserts.

Bhuyan, M. M., Surja, M. C., & Deb, U. K. (2024). Effect of Twist Ratios on Heat Transfer for Circular-Cut Twisted Tape Inserts in U-Shaped Pipe. *International Journal of Heat & Technology*, *42*(6). 1952-1962. 10.18280/ijht.420612.

Bhuyan, M., Surja, M. C., & Deb, U. K. (2025). Numerical Study on Heat Transfer Enhancement Using Rectangular Modified Cut Twisted Tape Inserts in Tubular Pipes. *Journal homepage: http://iieta. org/journals/ijht*, *43*(3), 873- 886.

Cook, R. D. (1995). *Finite element modeling for stress analysis*. Wiley.

Esarte, J., Min, G., & Rowe, D. M. (2001). Modelling heat exchangers for thermoelectric generators. *Journal of Power Sources, 93*, 72–76.

Hardt, S., Ehrfeld, W., & Hessel, V. (2003). Strategies for size reduction of microreactors by heat transfer enhancement effects. *Chemical Engineering Communications, 190*, 540–559.

Jia, R., Hu, J., & Elbalsohi, A. E. M. (2014, April 3–5). Analysis of a counter flow parallel-plate heat exchanger. In *ASEE 2014 Zone I Conference*. University of Bridgeport, Bridgeport, CT, USA.

Jia, R., Hu, J., & Xiong, X. (2014, October). Modeling of a counter flow plate fin heat exchanger. In *Proceedings of the 2014 COMSOL Conference*. Boston, MA, USA.

Löhner, R. (1987). An adaptive finite element scheme for transient problems in CFD. *Comput. Methods Appl. Mech. Eng., 61*, 323–338.

Marquardt, E. D., & Radebaugh, R. (2003). Compact high effectiveness parallel plate heat exchangers. In R. G. Ross Jr. (Ed.), *Cryocoolers* (Vol. 12, pp. 507–516). Kluwer Academic/Plenum Publishers.

Nellis, G. F. (2003). A heat exchanger model that includes axial conduction, parasitic heat loads, and property variations. *Cryogenics, 43*, 523–538.

Nunge, R. J., & Gill, W. N. (1966). An analytical study of laminar counterflow double-pipe heat exchangers. *AIChE Journal, 12*, 279–289.

Onufrena, A., Koettig, T., Bremer, J., Tirolien, T., Dorau, T., Laguna, M. B., & ter Brake, H. J. M. (2022). Design of a compact mesh-based high-effectiveness counter-flow heat exchanger and its integration in remote cooling system. *International Journal of Heat and Mass Transfer, 183*, 122107. https://doi.org/10.1016/j.ijheatmasstransfer.2021.122107

Papoutsakis, E., & Ramkrishna, D. (1981). Conjugated Graetz problems. I. General formalism and a class of solid-fluid problems. *Chemical Engineering Science, 36,* 1381–1390.

Papoutsakis, E., & Ramkrishna, D. (1981). Conjugated Graetz problems. II. Fluid-fluid problems. *Chemical Engineering Science, 36,* 1393–1399.

Perelman, T. L. (1961). On conjugated problems of heat transfer. *International Journal of Heat and Mass Transfer, 3,* 293–303.

Piroozfam, N., Hosseinpour Shafaghi, A., & Razavi, S. E. (2018). Numerical investigation of three methodsfor improving heat transfer in counter-flow heat exchangers. *International Journal of Thermal Sciences, 133,* 230–239. https://doi.org/10.1016/j.ijthermalsci.2018.07.033

Radebaugh, R. (2005). Microscale heat transfer at low temperatures. In S. Kakac et al. (Eds.), *Microscale heat transfer – fundamentals and applications* (pp. 93–124). Springer.

Shah, R. K., & London, A. L. (1978). *Laminar flow forced convection in ducts: A source book for compact heat exchanger analytical data* (pp. 196–207). Academic Press.

S. Acherjee, U. K. Deb, M. M. Bhuyan, The effect of the angle of perforation on perforated inserts in a pipe flow for heat transfer analysis, *Mathematics and Computers in Simulation*, Volume 171, 2020, Pages 306-314, ISSN 0378-4754, https://doi.org/10.1016/j.matcom.2019.10.003.

Wakeland, R. S., & Keoliana, R. M. (2004). Effectiveness of parallel-plate heat exchangers in thermoacoustic devices. *Journal of the Acoustical Society of America, 115,* 288–2873.

Yu, J., & Zhao, H. (2007). A numerical model for thermoelectric generator with the parallel-plate heat exchanger. *Journal of Power Sources, 172,* 428–434.

Zavala-Río, A., & Santiesteban-Cos, R. (2004). Qualitatively reliable compartmental models for double-pipe heat exchangers. In *Proceedings of the 2nd IFAC Symposium on System, Structure, and Control* (pp. 406–411). Oaxaca, Mexico.